International Journal of Material Forming (2018) 11:789–805
https://doi.org/10.1007/s12289-017-1388-x

ORIGINAL RESEARCH

Contact geometry estimation and precise radial force prediction for the radial-axial ring rolling process

Luca Quagliato[1] · Guido A. Berti[1] · Dongwook Kim[2] · Naksoo Kim[2]

Received: 24 January 2017 / Accepted: 13 November 2017 / Published online: 13 December 2017

Abstract In the present research work, the modular parametric design plug-in Grasshopper, available in Rhinoceros 5, is utilized as a pre-processor for the estimation of the projection of the contact length between ring and tools in the radial-axial ring rolling process. The estimated lengths, for each round of the process, are then used in a slip line based force model for the precise estimation of the radial forming force. The proposed method allows reducing the inaccuracies of the traditional approaches since it supersedes the concept of common thickness draft on both mandrel and main roll side, allowing a more precise estimation of the projection of the contact arc between ring and tools, considered to have a unique value on both mandrel side and main roll side. The fulfillment of this last assumption ensures the forming force to have the same value regardless it is calculated on the mandrel side or on the main roll side. The model has been validated by cross-comparing the analytical results with those of laboratory experiment and finite element simulation. The developed analytical model has been also applied to three different study cases where the previous literature models for the calculation of the projection of the contact arc have shown inaccuracies, demonstrating that the proposed approach can overcome these limitations. The positive cross comparisons among laboratory experiment, FEM simulations, and analytical estimations prove the reliability of the proposed approach, as well as its good integration with authors' previous analytical algorithms.

Keywords Ring rolling · Contact geometry · CAD-analytical approach · Force prediction

Introduction

Thanks to the wide range of applications, as well as for its important features such as short cycle time, high energy-efficiency, favorable grain orientation, and versatility [1], radial-axial ring rolling, Fig. 1, has become a highly widespread metal forming process. The ring rolling process design phase, as well that of all manufacturing processes, is a critical stage where the mutual interaction among workpiece blank dimensions, material properties, process conditions, and parameters must be taken into account simultaneously. During the design phase, process engineers should make some preliminary calculations in order to identify the ring rolling mill to utilize for the realization of the ring. To this aim, one of the most important parameter for a proper choice of the ring rolling machine is the maximum forming force required during the process. As for the calculation of the forming force, finite element method (FEM) simulations are a useful approach that allows a good estimation of several forming parameters but their utilization is normally characterized by a huge computational time, due to the high number of elements composing the mesh domain. On the other hand, if a coarse mesh is utilized, aiming to reduce the computational time, the quality of the estimation turns to be very poor and may lead to severe under- or over-estimation of the process output variable (such as geometry and forming forces).

In the literature, several authors focused their effort on the estimation of the radial forming force in the radial-axial ring rolling process, utilizing different technics and approaches, as hereafter summarized. The FE methodology has been utilized, by Zhou et al. [2], for the analysis of the variation of the radial forming force in case of different main roll diameters, and by Guo et al. [3] for the validation of a stable forming conditions model.

Moreover, Kim et al. [4] and Yea et al. [5], by utilizing a spatially fixed mesh approach, developed a specific FEM software for the analysis of the ring rolling process, whose results

✉ Naksoo Kim
nskim@sogang.ac.kr

[1] Department of Management and Engineering, Padua University, Stradella San Nicola 3, 36100 Vicenza, Italy

[2] Department of Mechanical Engineering, Sogang University, 35 Baekbeom-ro, Daeheung-dong, Mapo-gu, Seoul, Republic of Korea

have shown good agreement with those of the relevant laboratory experiment.

Concerning the development of analytical models for the estimation of the process forces in the ring rolling process, Parvizi et al. [6] developed an analytical SLAB model for the estimation of the radial forming force and analyzed the influence of the contact arc length on that force. In addition to that, Parvizi et al. [7] also developed an upper bound force model but the comparison between analytical solution and laboratory experiments have shown an underestimation of the maximum forming force. In addition to that, Mamalis et al. [8] applied the slip line theory for the estimation of the forming pressure during the deformation showing that the resulting maximum forming force has a maximum error limited to 15%, in comparison to the relevant experiment. In [8], the pressure evolution during the deformation has been also analytically studied proving that its peak is closer to the onset of the deformation gap rather than to the exit.

Except for the FEM-based analysis, all the previously mentioned analytical force models include an estimation of the projection of the contact arc between ring and tools, which is one of the key parameters for the estimation of the radial forming force.

The models for the estimation of the projection of the contact length in the mandrel-main roll deformation gap are mainly due to Yang et al. [9], Qian et al. [10] and Parvizi et al. [6]. As it will be shown in the result section, although these literature models partially differ in terms of input parameters, their results turn to be very similar and their estimation of the projection of the contact arc have shown to share the same limitation. For this reason, a more precise approach to estimate the real contact geometry between ring and tools should be developed.

The present research work details a new mixed CAD-analytical approach which aims to precisely calculate, by utilizing a Boolean solid intersection function, the real projection of the contact arc between ring and tools in the deformation gap of the ring rolling process. The projection of the contact arc is inputted in a slip line-based force model for the accurate estimation of the radial forming force. The developed model, as well as the literature ones [6, 9, 10], are all purely-geometrical models those estimate the projection of the contact arc between the ring and the tool on the basis of their geometries in a specific instant of the process or, in other words, for a specific geometry of a portion of the ring.

In order to validate the proposed approach, a laboratory experiment on a ring rolling test machine has been carried out and the radial forming force during the process has been recorded by means of a load cell installed on the main roll tool. The cross-comparison among analytical, numerical and experimental results concerning the radial forming force have shown good agreement, allowing to prove the reliability of both analytical and numerical models.

Afterward, aiming to prove that the proposed approach can supersede the limitations of the previous literature models, three study cases have been taken into account. In these three cases, if the projection of the contact arc between ring and tools is estimated by utilizing the literature models [6, 9, 10] the resulting radial forming force is strongly underestimated (the error can reach up 23.7%, in comparison to the relevant FE simulation). However, if the proposed approach is utilized, the error in the estimation of the maximum radial forming force is limited to a ± 3% range, showing the improvement of the proposed approach in comparison to the previous literature ones.

Contact geometry estimation utilizing grasshopper

The Rhinoceros 5 "Grasshopper" plug-in [11, 12] is a useful blocks-programmable tool, which helps to create parametric geometries, based on input geometrical variables and on command blocks. In the developed mixed CAD-analytical model, the Grasshopper program is utilized for the calculation of the projection of the contact arc between tools and ring in the mandrel-main roll deformation gap and the detailed explanation of the calculation procedure is presented in this paragraph of the paper.

The algorithm for the estimation of the contact geometry proposed in this paper is subdivided into six sections, as shown in Fig. 2. The core of the developed algorithm is represented by "Contact geometry estimation utilizing grasshopper" section to "Models implementation" section. Concerning the remaining two sections, "Introduction" section represents the calculation of the input parameters for the algorithm, operated by utilizing authors' previous work [13] whereas "Model validation" section is the part of the calculation where the results of the algorithm are collected together and utilized

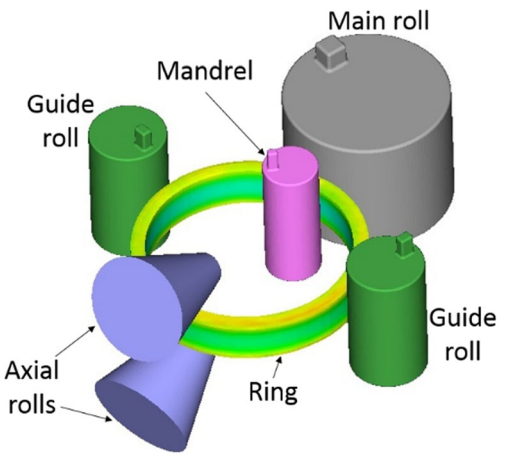

Fig. 1 Radial-axial ring rolling (schematic representation)

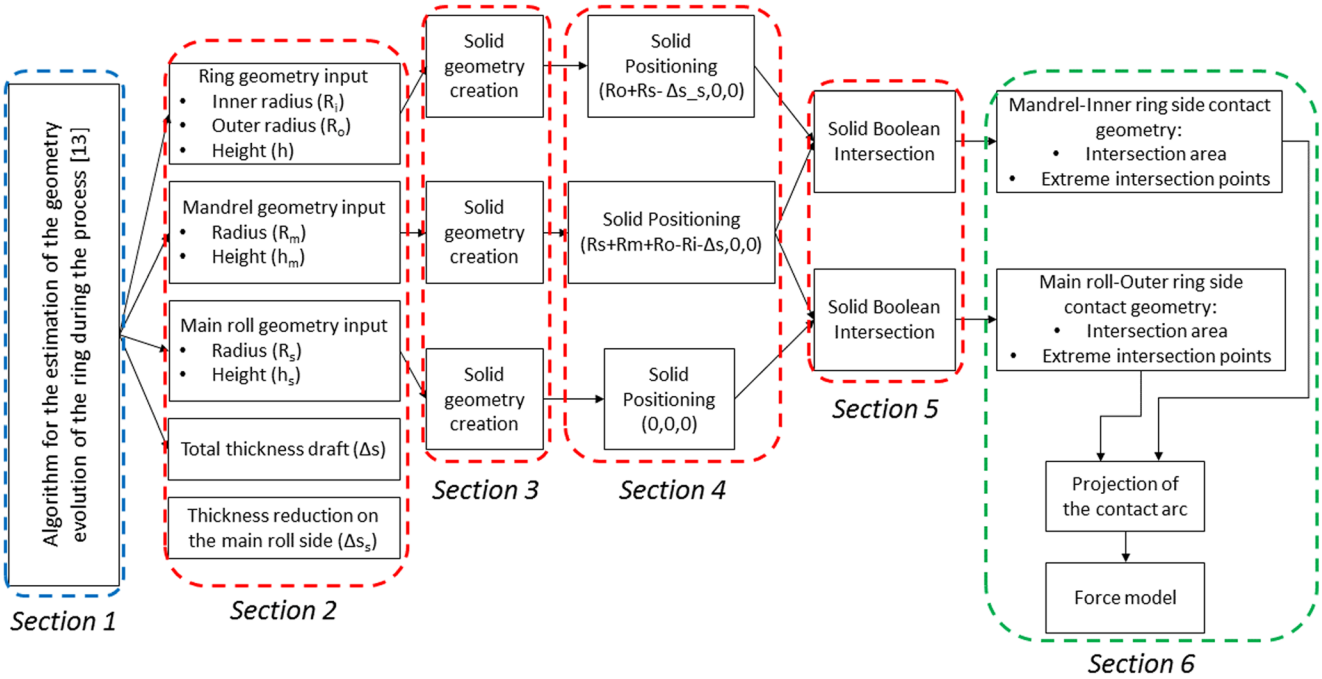

Fig. 2 Algorithm module-block implementation

for the estimation of the forming force in the mandrel-main roll deformation gap.

Geometry input data and geometry building section

The input parameters for the Grasshopper module block algorithm, "Introduction" section, are derived from authors' previous work [13], where an analytical model for the estimation of the evolution of the geometry of the ring was proposed and validated. The geometry estimation algorithm, detailed in [13], receives as input the following data: the geometries of the ring (initial and final), the geometry of the ring rolling mill and the motion laws of the tools (mandrel, main roll, and axial rolls) and returns as output the evolution of the ring dimensions throughout the process.

By utilizing the algorithm proposed in [13], the initial ring, namely the ring blank shown in Fig. 3a, is subdivided into a chosen number of slices, as shown in Fig. 3b and, accordingly, the geometry of each slice is estimated throughout the process. At the beginning of the process, each slice of the ring has the same dimensions both on its left and right faces whereas during the expansion phase, due to the incremental nature of the ring rolling process, left and right face of each slice will have different dimensions, namely different inner radius, outer radius, and height, as shown in Fig. 3c. The geometry of each slice will vary, according to its relevant position in the ring and

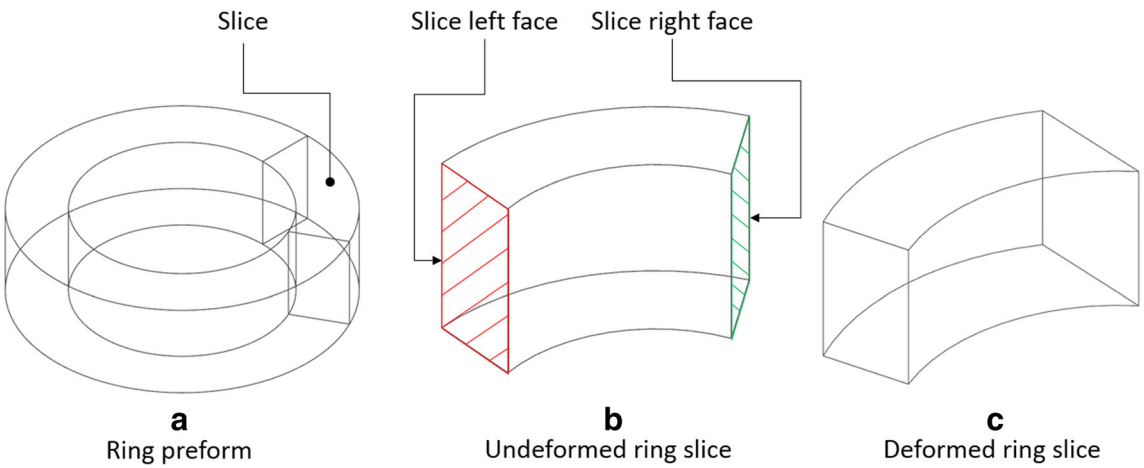

Fig. 3 Ring blank geometry (**a**), ring slice geometry from the ring blank (**b**) and deformed ring slice (**c**)

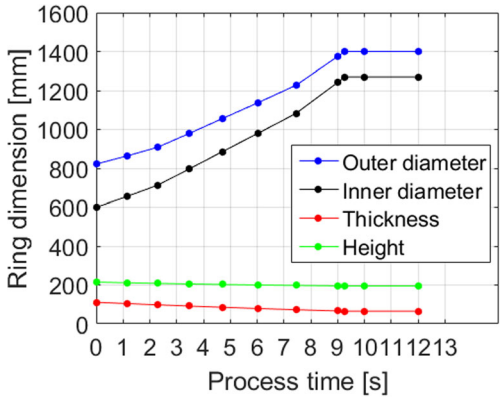

Fig. 4 Ring geometry prediction throughout the process

it depends on the motion rules of mandrel, main roll, upper and lower axial rolls.

From the dimensions of left and right face of each slice of the ring, Fig. 3b, its average geometry is calculated according to (1) and the relevant parameters, namely inner radius R_i, outer radius R_o, and height h, are utilized in the "Ring geometry input" block in "Contact geometry estimation utilizing grasshoppher" section, Fig. 2.

$$\begin{aligned} R_i &= \left(R_{i,LF} + R_{i,RF}\right)/2 \\ R_o &= \left(R_{o,LF} + R_{o,RF}\right)/2 \\ h &= \left(h_{LF} + h_{RF}\right)/2 \end{aligned} \tag{1}$$

In Eq. (1), $R_{o,\,LF}$, $R_{i,\,LF}$, $R_{o,\,RF}$, $R_{i,\,RF}$ stand for the outer and inner radii of the left face and those of the right face, respectively. Considering the contribution of each slice, in terms of its geometry and its relevant position in the ring, the real geometry of the ring can be reconstructed allowing to calculate the evolution of inner radius, outer radius, thickness and height throughout the process, as reported in the example of the algorithm output shown in Fig. 4.

As proven in [13, 14], the subdivision of the ring into slices allows a more precise estimation of the geometrical evolution of the ring throughout the process and, as discussed in [14], a reasonable compromise to limit the complexity of the calculation, while granting accurate results, is to set the discretization angle to 10 degrees, meaning to subdivide the ring into 36 slices. The influence of the number of slices in which the ring is subdivided over accuracy and computational time is discussed in the models implementation, "Model implementation" section, of the paper.

For each slice into which the ring has been subdivided and for each round of the process, the geometry data are inputted in the algorithm, "Contact geometry estimation utilizing Grasshopper" section in Fig. 2, and utilized for the estimation of the contact geometry between ring and tools.

In addition to that, in "Contact geometry estimation utilizing Grasshopper" section, the geometry of main roll and mandrel, in terms of their diameters, namely R_s (main roll radius) and R_m (mandrel radius), and heights, namely h_s (main roll height) and h_m (mandrel height), are inputted and considered as constant throughout the process. Tools and ring parameters are defined as shown Fig. 5.

In order to complete the input required for "Contact geometry estimation utilizing Grasshopper" section, the total thickness reduction for the considered slice in the considered round of the process and the amount of thickness reduction on the main roll side must be inputted in the algorithm. The total amount of thickness draft, $\Delta s = s_0 - s_F$, is calculated according to the relative distance between mandrel and main roll in the moment when the slice is passing through the deformation gap. The amount of thickness reduction on the main roll side,

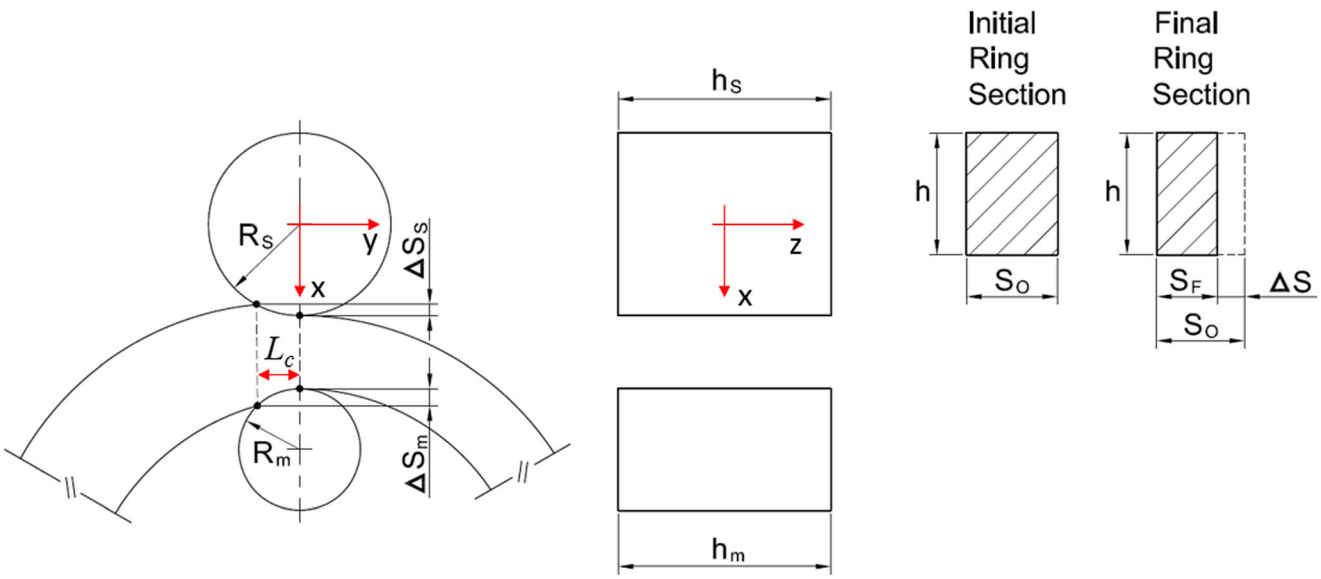

Fig. 5 Parameters definition in the contact geometry between ring and tools

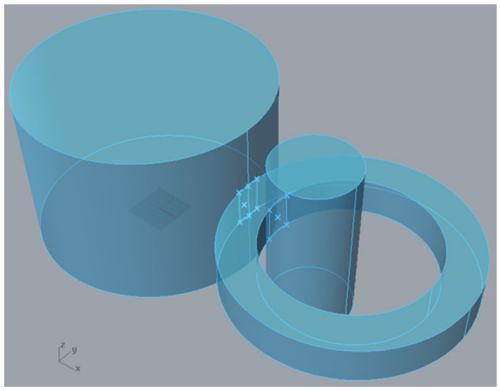

Fig. 6 Rhinoceros 5 output geometry

Δs_s, is considered as a variable in the algorithm and its calculation is based on the assumption that the projection of the contact arc on the mandrel side and on the main roll side have the same value, as shown in Fig. 5. This assumption has been considered also in previous works related to the ring rolling process, namely in Parvizi et al. [6, 7] and in Yang et al. [9]. In [9], it has been proven that, since the difference in the thickness draft in the mandrel side and in the main roll side is small in comparison to the thickness of the ring, considering a common projection for the contact arc is an acceptable approximation. Considering this assumption, the roll force on the mandrel side and on the main roll side will have the same value.

In the computations operated in the algorithm, the user sets the initial value for the thickness reduction on the main roll side, Δs_s, and the algorithm automatically varies it until the projection of the contact arc assume the same values, on both tools sides. This value is considered the result of the algorithm, related to "Model validation" section of the algorithm, as shown in Fig. 2.

At the end of "Contact geometry estimation utilizing Grasshopper" section, the sections of ring, mandrel and main roll are generated in the x-y plane and in "Literature models for the calculation of the projection of the contact arc length" section they are extruded along the z-direction, in order to obtain the solid geometries. At this point, only the main roll geometry is located in the right position (origin of the coordinate system), but mandrel and ring must be located in the right positions with respect to the main roll and according to the considered round of the process. The positioning strategy, task relevant for "Slip line force model" section of the algorithm, is explained in the following paragraph.

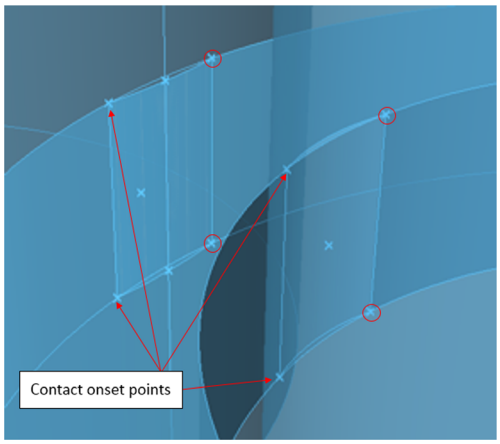

Fig. 7 Detail of the extremum contact points

Table 1 Nomenclature for the force models parameters

Parameters	Description
R_s	Main roll radius
R_m	Mandrel radius
s_0	Thickness of the ring at the onset of the deformation gap
s_F	Thickness of the ring at the exit of the deformation gap
Δs	$s_0 - s_F$ (Thickness draft)
R_o	Outer radius of the ring at the exit of the deformation gap
R_i	Inner radius of the ring at the exit of the deformation gap
R_{avg}	Average radius of the ring at the exit of the deformation gap

Geometry positioning section

Once the solid geometries have been generated ("Literature models for the calculation of the projection of the contact arc length" section of the algorithm), in order to properly calculate the Boolean intersection among solids, they must be positioned in the right location for the considered round of the process. "Slip line force model" section, Fig. 2, handles the positioning operations and the objects to locate are the ring and the mandrel. The ring is positioned considering that its y-coordinate must be zero (aligned with the main roll y-axis)

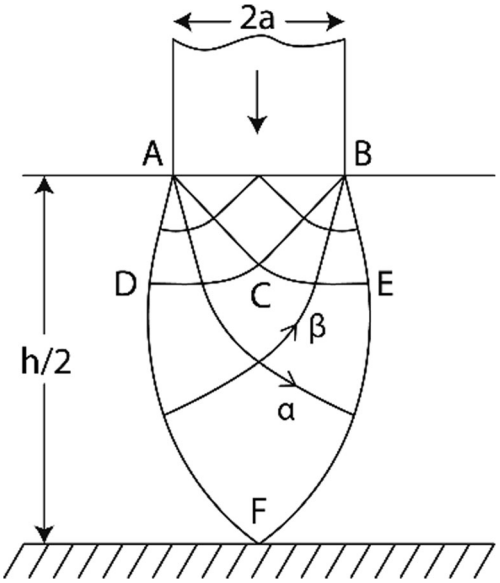

Fig. 8 Hill's slip line flat indenter solution [15] (contact geometry)

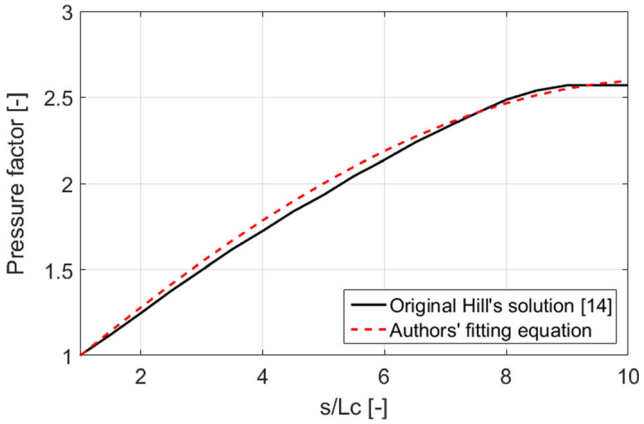

Fig. 9 Pressure factor chart, comparison between original Hill's solution and authors' fitting

whereas, along the z-axis, the ring center must be aligned with the center of the main roll, along the z-direction. The x-coordinate of the ring is defined according to the amount of draft on the main roll side, as shown in following Eq. (2), where R_o is the average outer radius of the considered ring section, R_s is the radius of the main roll and, as pointed out before, Δs_s is the amount of thickness draft on the main roll side.

$$x_R = R_o + R_s - \Delta s_s \tag{2}$$

Concerning the position of the mandrel, its maximum z-coordinate must be aligned with the maximum one of the main roll, its y-coordinate is also aligned with y = 0 (center of the main roll in this direction) whereas the x-coordinate is controlled by the thickness draft in the mandrel side. Having set the thickness draft in the main roll side as a variable parameters, the thickness draft on the mandrel side is defined as $\Delta s_m = \Delta s - \Delta s_s$and, accordingly, the x-coordinate of the center of the mandrel can be calculated according to Eq. (3).

$$x_m = R_s + R_m + R_o - R_i - \Delta s \tag{3}$$

In Eq. (3), R_m is the radius of the mandrel, R_i is the average inner radius of the considered ring slice, in the considered round, and Δs the total amount of thickness draft in the considered slice in the considered round of the process.

Table 2 Pressure factor equation coefficients

Parameters	Value
p_1	−0.00048
p_2	−0.00697
p_3	0.30764
p_4	0.69656

Table 3 42CrMo4 alloy material model ranges and constants

Parameters	Value
Temperature range for the model [°C]	800–1250
Strain range for the model [−]	0.05–2
Strain rate range for the model [1/s]	0.01–150
C_1	5290.47
C_2	−0.0036967
n_1	−0.000334025
n_2	0.20612
L_1	−8.26584e-5
L_2	0.0289085
m_1	0.000300752
m_2	−0.156181

Boolean geometry intersection and contact length calculation

At this point of the calculation, all 2D geometries have been created, extruded along the z-direction and located in the right position considering a specific slice of the ring in a specific instant of the process. The geometries data and the relevant position are now fed to "Model implementation" section, Fig. 2, where the Boolean intersection between the outer area of the ring and the main roll and between the inner area of the ring and the mandrel are carried out, as shown in Fig. 6. The Boolean intersection allows determining the contact area as well as the extremum points of contact ("Model validation" section), on both main roll side and mandrel side, Fig. 7.

As previously anticipated, the chosen criteria to calculate a unique solution is to consider the projection of the contact arc between tools and ring to have the same value on both main roll and mandrel side. By applying this assumption, the algorithm varies Δs_s until the coordinate of the extremum points of contact have the same value on both sides. Being the center of main roll, mandrel, and ring aligned along the y-axis, the y-coordinates of the extreme points on the left side of Fig. 7 automatically define the projection of the contact arc between ring and tools, output of the algorithm. In Fig. 7, the contact points surrounded by a red circle are automatically created by the Rhinoceros 5 program but are not considered in the calculation since they are outside the deformation gap.

In paragraph 3 of the paper, a literature survey of the model available in the literature for the estimation of the projection of the contact arc is presented. In the result section of the paper, a comparison of the radial forming force obtained by utilizing the proposed approach and those calculated by means of the three literature models is presented, allowing to prove the improvement given by the proposed methodology in comparison to those available in the literature.

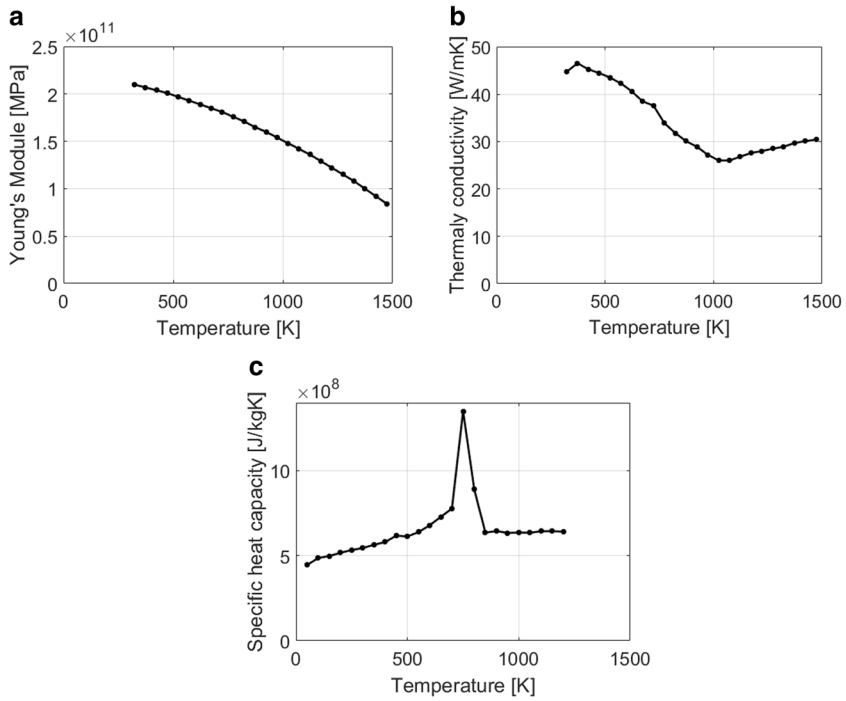

Fig. 10 **a** Young's modulus of 42CrMo4 steel. **b** Thermal conductivity of 42CrMo4 steel. **c** Specific heat capacity of 42CrMo4 steel

Algorithm calculation procedure

The CAD-analytical approach presented in this paper utilizes the ring slice as reference element for the calculation. For each round of the process, the value of the projection of the contact arc between ring and tools is estimated for each slice into which the ring has been initially subdivided. As detailed in previous authors' work [13], at the beginning of the process, the ring is subdivided in a certain amount of slices, according to a user choice, and the evolution of the geometry of each slice is estimated throughout the process. The geometry of the considered slice is inputted in the algorithm presented in this paper and both rings and tools are aligned in order to reproduce their position, with respect to the considered slice, in a specific instant of the process. The inputted geometry is that of one slice and, in the CAD ambient, the ring is modeled as an annular shape with the dimensions, namely diameters and height, of the considered slice.

Afterward, the user is asked to input the initial guess for the value of the thickness reduction on the main roll side, namely Δs_s. Based on a secant method-based convergence algorithm, Δs_s is varied utilizing the difference between the projection of the contact arc between ring and tools, both on the mandrel side and main roll side, as convergence criterion. When the two projections have the same value, the corresponding Δs_s is considered as the final solution for the thickness reduction on the main roll side and, accordingly, the thickness reduction on the mandrel side is calculated.

The procedure is repeated for each slice of the ring and for each round of the process and the average values of the contact arc between ring and tools, for each round of the process, are estimated by averaging that of each slice. Therefore, for each round of the process, for all the n-number of slices, the projection of the contact arc is estimated and their average values, one for each round of the process, are utilized for the calculation of the radial forming force, following the procedure detailed in paragraph 4 of the paper.

Table 4 Initial and final geometries and mandrel feeding speed for the numerical study cases

	Ring initial geometry [mm]			Ring final geometry [mm]			Mandrel feeding speed [mm/s]	
Case	Outer diam.	Inner diam.	Height	Outer diam.	Inner diam.	Height	Initial	Final
1	518.9	325.00	195.4	800.0	680.0	180.0	7.7	6.0
2	550.9	325.00	175.4	800.0	645.0	145.0	7.5	5.0
3	574.5	325.00	124.8	800.0	600.0	100.0	6.0	4.5

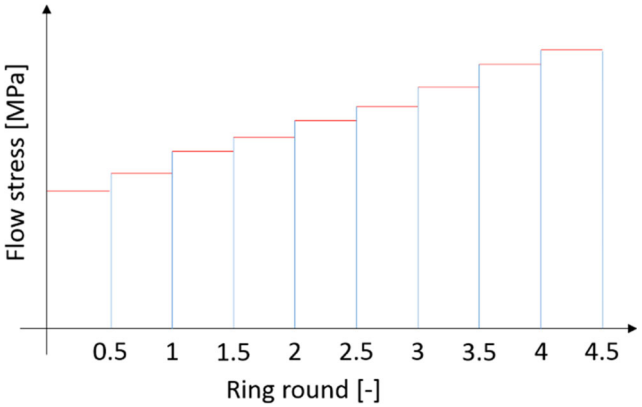

Fig. 11 Update of the flow stress of the material for increasing number of ring rounds

Literature models for the calculation of the projection of the contact arc length

Previous estimations of the contact geometry between ring and tools in the mandrel-main roll deformation gap are based on simplifications, especially concerning the estimation of the projection of the contact arc between ring and tools. Consequently, as it will be shown in the result section, in some case, the utilization of previous literature models lead to an underestimation of the radial forming force.

In the literature, many contributions concerning the contact geometry estimation in the ring rolling process, in terms of formulation for the estimation of the projection of the contact arc between ring and tools in the mandrel-main roll deformation gap, Fig. 1, have been formulated. The proposed equations: Yang et al. [9], Qian et al. [10] and Parvizi et al. [6] are reported in Eqs. (4)–(6) respectively. The terminology is listed and explained in the following Table 1. The variation of thickness between the onset and the exit of the deformation gap is defined as $\Delta s = s_0 - s_F$ whereas the average radius of the ring as $R_{avg} = (R_o + R_i)/2$.

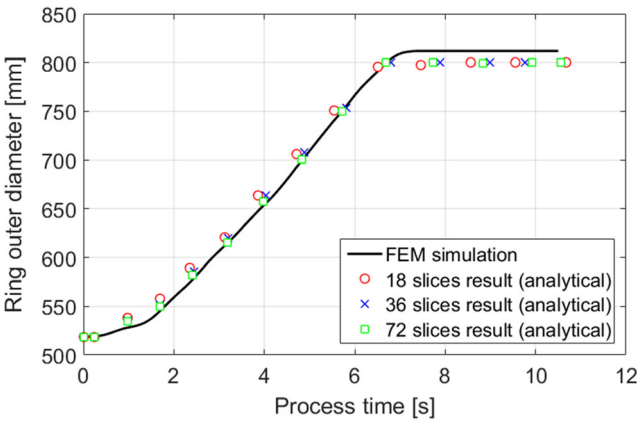

Fig. 12 Prediction of the outer diameter of the ring for different number of slices, in comparison to the relevant numerical simulation

$$L_{c-Y} = \sqrt{R_s^2 - \left[\frac{(R_{avg} + s_0/2)^2 - (R_s + s_1/2 + R_{avg})^2 - R_s^2}{2(R_s + s_1/2 + R_{avg})}\right]^2} \tag{4}$$

$$L_{c-Q} = \sqrt{\frac{2\Delta s}{(1/R_s) + (1/R_m) + (1/R_o) - (1/R_i)}} \tag{5}$$

$$L_{c-P} = \sqrt{R_s^2 - \left[\frac{(R_s + R_m - \Delta s)^2 + R_s^2 - R_m^2}{2(R_s + R_m - \Delta s)}\right]^2} \tag{6}$$

In the result section, these three models as well authors combined CAD-analytical model are applied to three different study cases in order to show that: i) the results obtainable with these three models are very similar to each other and ii) that the developed approach allows overcoming their limitations, resulting in a better estimation of the projection of the contact arc between ring and tools, confirmed by a more precise calculation of the radial forming force.

In the following paragraph of the paper, the force model utilized in the validation case as well as in all the study cases is presented and explained, highlighting the importance of the projection of the contact arc length in the calculation of one of the force model parameter, namely the pressure factor.

Slip line force model

As concerns the model for the calculation of the forming force, authors' have chosen to utilize the Hill's slip line flat indenters force model detailed in [15] and developed for the case of a flat punch indenting on a flat surface, Fig. 8. Since this model is based on a straight contact surface between the workpiece and the tool, by considering the projection of the contact arc, and not its curved geometry, the contact assumption is fulfilled.

According to Hill's slip line model [15], the force is proportional to a pressure factor, here expressed by the symbol γ, and which represents the state of stress in the plastically deformed region. The pressure factor is proportional to the ratio s/L_c, namely the ratio between the thickness of the ring slice undergoing the deformation and the projection of contact length, assumed to be a straight line. The slice of the ring undergoing the deformation is considered to have a constant thickness before the deformation, s_0, and to reach a constant final thickness s_F after it has exited from the deformation gap. The thickness before the deformation is determined by the distance between mandrel and main roll in the previous round of the process whereas that after the deformation by the distance between mandrel and main roll in the present round. Both estimations are derived by utilizing authors' previous work [14].

Table 5 Accuracy in the prediction of the outer diameter of the ring for different number of slices

Process time FEM [s]	0	0.25	0.97	1.70	2.41	3.18	3.96	4.81	5.69	6.67	7.69	8.80	9.75	10.59
FEM simulation results [mm]	518.95	519.19	528.03	545.56	577.32	614.56	652.48	698.49	748.66	798.50	811.75	811.75	811.75	811.75
Process time 18 slices (analytical) [s]	0	0.25	0.97	1.70	2.36	3.13	3.86	4.72	5.54	6.515	7.45	8.57	9.560	10.68
18 slices (analytical) [mm]	518.84	518.84	538.48	558.11	589.53	620.95	663.49	706.03	750.93	795.84	797.92	800.00	800.00	800.00
% Error 18 slices (analytical)	−0.02%	−0.07%	1.98%	2.30%	2.12%	1.04%	1.69%	1.08%	0.30%	−0.33%	−1.70%	−1.45%	−1.45%	−1.45%
Process time 36 slices (analytical) [s]	0	0.25	0.97	1.70	2.44	3.21	4.04	4.89	5.82	6.804	7.89	8.99	9.773	10.55
36 slices (analytical) [mm]	518.85	518.84	535.11	551.37	585.71	620.04	663.82	707.59	753.79	799.89	800.00	800.00	800.00	800.00
% Error 36 slices (analytical)	−0.02%	−0.07%	1.34%	1.06%	1.45%	0.89%	1.74%	1.30%	0.69%	0.17%	−1.45%	1.45%	1.45%	1.45%
Process time 36 slices (analytical) [s]	0	0.25	0.97	1.70	2.42	3.18	3.98	4.83	5.72	6.695	7.73	8.83	9.92	10.55
72 slices (analytical) [mm]	518.85	518.85	534.19	549.53	582.22	614.92	657.83	700.74	750.37	799.75	799.81	799.61	799.81	800.00
% Error 72 slices (analytical)	−0.02%	−0.07%	1.17%	0.73%	0.85%	0.06%	0.82%	0.32%	0.23%	0.19%	−1.47%	−1.49%	−1.47%	−1.45%

Since the contact arc, in terms of its projection, is essential for the calculation of the pressure factor, its proper calculation plays an important role in the estimation of the radial forming force. As shown in Fig. 9, the pressure factor curve starts from 1, the pressure to start the plastic deformation, and ends with the value of 2.57, which is the limit over which the surface of the material is indented by the tool and the material is spread aside from the indenting area.

Based on Hill's graphical solution, authors have derived a third-order Eq. (7) to facilitate its utilization in the computation. Original and fitted curved are both shown in Fig. 9 whereas the coefficient for the interpolation polynomial equation are reported in Table 2.

In the research presented in this paper, the spreading effect of the ring in the z-direction occurring in the mandrel-main roll deformation gap is neglected, and only the theoretical dimensions of the ring, as calculated in [13], are considered.

$$\gamma_j = p_1\left(\frac{s_j}{L_{c,j}}\right)^3 + p_2\left(\frac{s_j}{L_{c,j}}\right)^2 + p_3\left(\frac{s_j}{L_{c,j}}\right) + p_4 \tag{7}$$

Once γ is calculated, the radial forming force can be directly derived multiplying it by the projected contact area, $L_{c,j}h_j$, and for the yield shear stress of the material, k_j, as shown in (8). The yield shear stress k_j is defined according to the von Mises yield criterion as $k_j = \sigma_{fs}/\sqrt{3}$.

$$F_{radial,j} = 2h_j\gamma_j L_{c,j}k_j \tag{8}$$

The subscript "j" in Eqs. (7) and (8) emphasizes the fact that the developed algorithm allows computing the radial forming force for each slice in which the ring has been initially subdivided and for each round of the process.

Table 6 Influence of the number of slices on the accuracy of the estimation of the projection of the contact arc and of the calculation of the radial forming force

	$t_{comp,\,CAD}$ [s]	$L_{c,\,CAD}$ (3rd round) [mm]	$L_{c,\,FEM}$ (3rd round) [mm]	$L_{c,\,CAD}$ vs $L_{c,\,FEM}$ deviation [%]	$F_{authors}$[kN]	F_{FEM} [kN]	$F_{authors}$ vs F_{FEM} deviation [%]
18 slices subdivision	44.28	49.55	45.84	8.09%	1374.7	1322.4	3.95%
36 slices subdivision	91.80	48.03	45.84	4.78%	1353.6	1322.4	2.36%
72 slices subdivision	182.16	47.51	45.84	3.64%	1349.3	1322.4	2.03%

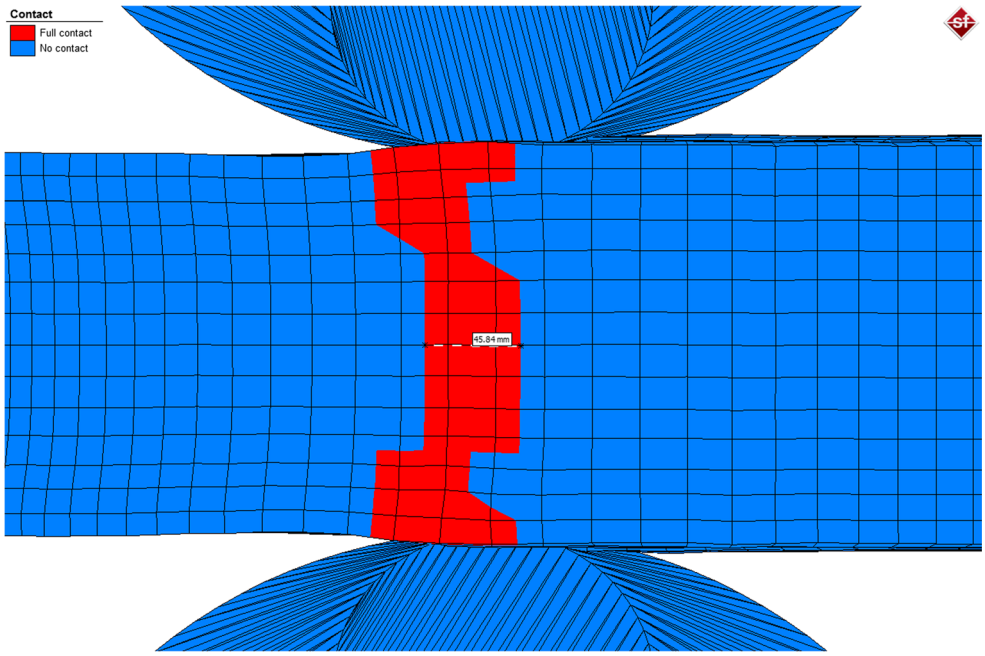

Fig. 13 Measurement of the projection of the contact arc between ring and tools

The factor "2" in Eq. (8) is given by the fact that the slip line force algorithm computes the forming force on one of the two sides, either on the mandrel side or on the main roll side. However, this force is that required to the slip line filed to reach half of the thickness of the ring. Since two symmetric slip line fields are drawn, one from the mandrel side and one from the main roll side and considering that this force has the same value, according to the chosen assumption that the projection of the contact arc is same on both sides, the factor "2" is introduced in (8) to calculate the total force.

The total force is the summation of that calculated from the slip line field on the mandrel side and that on the main roll side but, since they are equal according to the above-mentioned assumption, once one force is calculated it can be multiplied by "2" to obtain the total one.

Models implementation

The numerical models have been implemented in the commercial finite element software Simufact.Forming 12.03, largely utilized in many previous authors' works [13, 14, 16]. All the models have been meshed with hexahedral elements having the following dimensions: 16 mm (axial), 14 mm (radial) and 16 mm (tangential).

The mesh is composed of three-dimensional eight-node, isoparametric, arbitrarily distorted brick elements with trilinear interpolation (Marc® element type 7), associated with a three-dimensional, eight-node, first-order isoparametric, arbitrary quadrilateral element designed for three-dimensional heat transfer applications (Marc® element type 43). The element type 7 presents three degrees of freedom for each one of its nodes whereas the type 43 only one. According to Marc®

Fig. 14 Ring rolling test machine

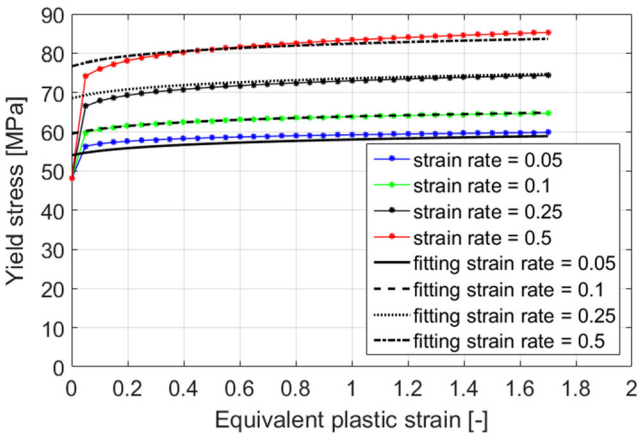

Fig. 15 Flow curves for Pb75-Sn25 alloy

Table 7 Pb75-Sn25 alloy material properties

Parameters	Value
Young's modulus	28 GPa
Poisson ratio	0.42
Density	9947.3 kg/m^3
Thermal conductivity	43 W/(mK)
Specific heat capacity	149.5 J/(kgK)
Thermal expansion	2.718E-5 (1/K)

user guide [17], element type 7 is particularly suitable for simulations where the contact is the predominant issue, such as in the case of ring-tools contact in the ring rolling process.

However, if the default trilinear interpolation function for the element type 7 and 43 is utilized, strains and thermal gradients are considered as constants throughout the element and, for element type 7, this fact can result in poor representation of shear and bending behaviors. For this reason, an alternative integration procedure, based on the constant dilatation method, has been set for the elements of the ring mesh in the developed numerical model. To this aim, the "EGEOM2" option field of the element type 7 has been set to "1", allowing to activate the constant dilatation option [18].

When the "EGEOM2" option is activated, the calculation of deviatoric and dilatational stresses and strains is split. The dilatational part accounts for the change in the element volume whereas the deviatoric part for the change in the element shape, respectively. The dilatational contribution is estimated with a reduced Gauss integration, allowing to avoid the volumetric locking issue, whereas the deviatoric contribution is evaluated by means of a full Gauss integration. By following this approach, the dilatation is correctly evaluated also in case of Poisson ratio close to 0.5, as in case of large plastic deformation.

The utilized solver is the MUMPS (MUltifrontal Massively Parallel sparse direct Solver) direct solver which performs a Gaussian factorization and is particularly indicated for the case of large dimensions, square, sparse matrixes. In all the numerical simulations, tool have been meshed as rigid with heat transfer.

In the numerical study cases, the rings are made of the 42CrMo4 steel alloy, frequently utilized for the production of rings in hot process conditions. The utilized flow stress model is shown in Eq. (9) whereas the constants for the relevant are listed in Table 3.

Table 8 Material model constants for Eq. (9)

Parameters	Value	Parameters	Value
K_0	92	b_0	0.015
a_0	0.1	b_1	0.17
a_1	0.03		

Table 9 Ring rolling test machine data, ring dimensions, and process conditions

Parameters	Value
Mandrel diameter	50 mm
Main roll diameter	200 mm
Axial rolls working plane length	190 mm
Axial rolls vertex angle	15.166 °
Guide rolls diameter	60 mm
Main roll rolling speed	0–60 rpm
Mandrel maximal pushing force	55 kN
Upper axial roll maximal pushing force	25 kN
Ring initial outer diameter	200 mm
Ring initial inner diameter	150 mm
Ring initial height	40 mm
Ring final outer diameter	232 mm
Ring final inner diameter	190 mm
Ring final height	39 mm
Ring initial temperature	20 °C
Mandrel initial feeding speed	0.23 mm/s
Mandrel final feeding speed	0.17 mm/s
Process time	33 s

$$\sigma_{fs} = C_1 e^{(C_2 \cdot T)} \varepsilon^{(n_1 \cdot T + n_2)} e^{\left(\frac{L_1 \cdot T + L_2}{\varepsilon}\right)} \dot{\varepsilon}^{(m_1 \cdot T + m_2)} \quad (9)$$

Equation (9) is the GMT-MATILDA® material equation, derived from the well-known Hansel-Spittel model [19]. Material equations constants, Table 3, together with material properties (Fig. 10a, b and c) are derived from the MATILDA® Material Information Link and Database Service) archive, available in the material database of Simufact.Forming 12.03.

The initial and final geometry of the ring, as well as the initial and final mandrel feeding speed relevant for the three numerical study cases, are reported in Table 4.

The same material equation, model constants, and material properties have been used in both FE simulations and analytical model in order to ensure a correct comparison among the results.

As concerns the mandrel, the velocity has been set up according to the motion law proposed in [13], following a linearly decreasing function from the beginning to the end of the forming process.

Friction has been accounted for by utilizing a shear stress friction model, Eq. (10), setting the friction factor to $m = 0.85$ for the contact between the ring and both the mandrel and the main toll and to $m = 0.6$ for the contact between the ring and

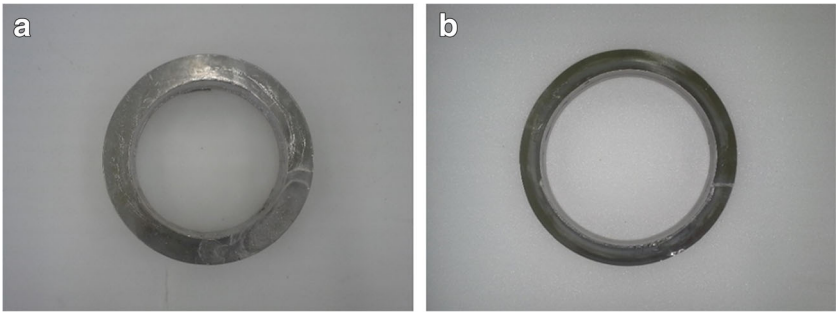

Fig. 16 **a** Pb-Sn ring preform. **b** Pb-Sn final ring

both axial rolls and centering rolls. The same friction factors have been utilized both in the numerical simulations and for the setting of the analytical model.

$$m = \frac{\tau_i}{k} \tag{10}$$

Concerning the update of the flow stress of the material in the analytical model, the procedure is hereafter detailed. At the beginning of the process, the entire ring is at the initial temperature of 1200 °C thus, according to Eq. (9), its initial flow stress can be calculated. Afterward, by utilizing the authors' previous models for the estimation of the strain [14], strain rate and temperature [16], the relevant parameters, namely the equivalent plastic strain, the equivalent plastic strain rate and the average temperature of the ring, are estimated for each half-round of the process. These estimations are inputted in Eq. (9) allowing to analytically estimate the flow stress of the material throughout the process, on a half-round based interval, as shown in Fig. 11.

For the considered half-round of the process, the material is considered to have a perfect-plastic behavior, which is updated after each half-round based on the new estimations of the strain, the strain rate, and the temperature. Since the estimations of strain, strain rate, and temperature, according to author' models [14, 16], are carried out on the final geometry of each slices at the exit of the deformation gaps, the estimated flow stresses are those at the final hardening value reached at the end of the relevant deformation. Following this rationale, the consideration of a perfect-plastic material behavior is in favor of safety. According to the estimation of the flow stress, by means of the von Mises yield criterion, the yield shear stress k_j required in the force model Eq. (8) is calculated. Since all the previous authors' analytical model are slice-based, the yield shear stress k_j is calculated for each slice of the ring and for each round of the process.

Although the subdivision of ring into slices is not the main topic of this research work, the number of slices in which the ring is subdivided influences both the accuracy of the geometrical data utilized as input for the CAD-analytical algorithm the total computational time. For this reason, the influence of the number of slices on the computational time and accuracy of the input variable for "Contact geometry estimation utilizing Grasshopper" section, Fig. 2, as well as on the computational time of the CAD-analytical model are hereafter discussed.

As previously mentioned, the input parameters for the CAD-analytical model proposed in this paper are obtained from authors' previous model [13]. In Fig. 12, the comparison in the estimation of the outer diameter of the ring when it is

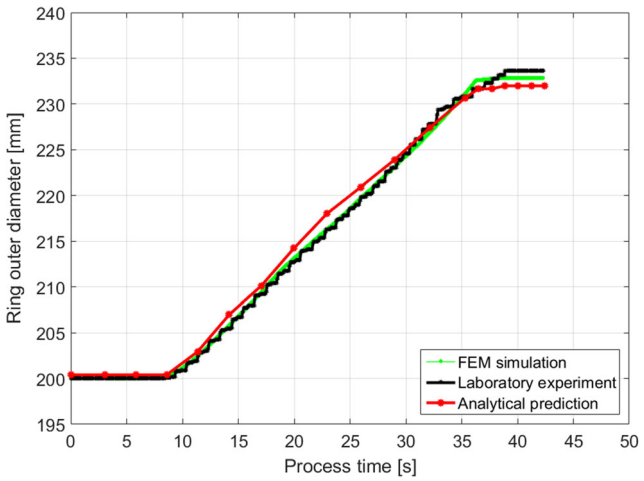

Fig. 17 Ring outer diameter expansion (results comparison)

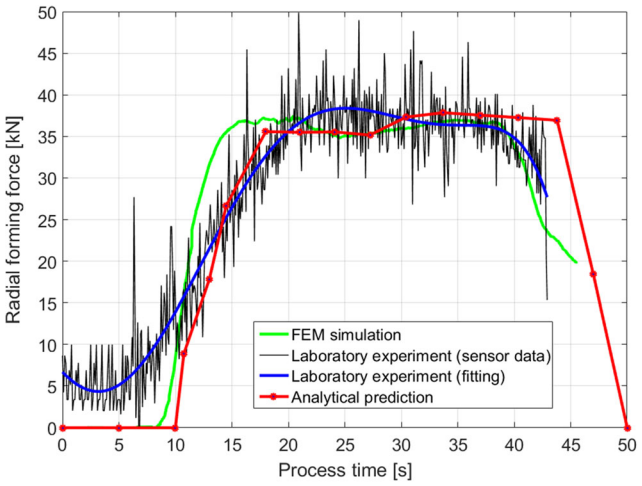

Fig. 18 Mandrel forming force results comparison

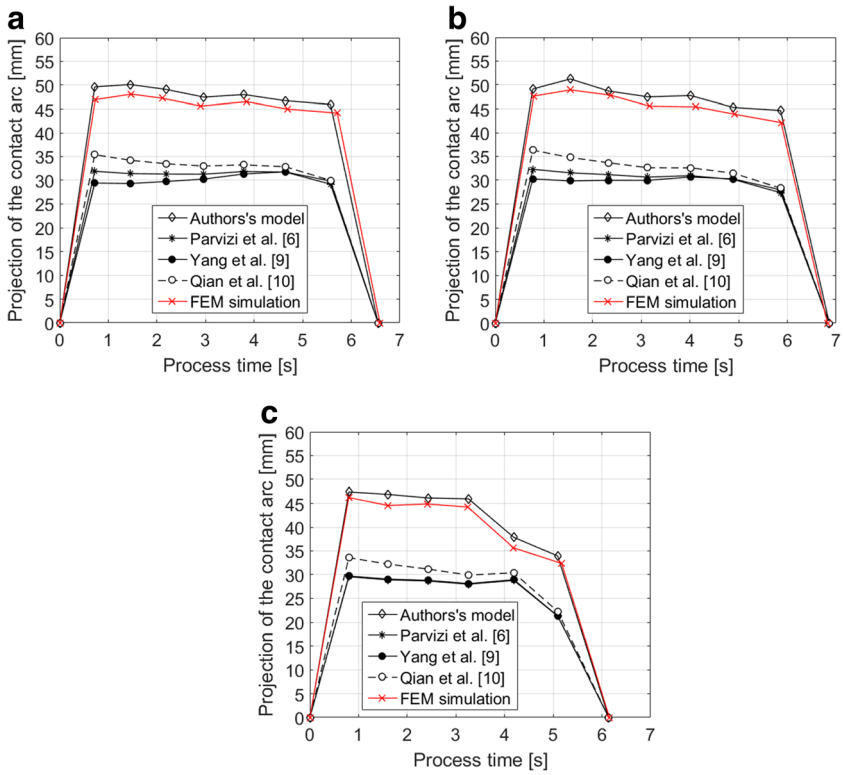

Fig. 19 Evolution of the projection of the contact arc calculated utilizing the literature models [6, 9, 10] and authors' model for case 1 (**a**), case 2 (**b**) and case (3)

subdivided in 18, 36 and 72 slices, for the study case 1 of Table 4, is reported.

Since the time steps of the numerical simulation are smaller than the calculation times in the analytical model, the results comparison is carried out at the simulation time steps closest to the analytical estimation times. The cross-comparison between numerical simulation results and analytical estimations carried out considering to subdivide the ring into 18, 36 and 72 slices, is reported in Table 5.

The small differences in the time instants at which the analytical model estimates the values of the outer diameter of the ring for the three slices configurations, Fig. 12, are given by the internal calculations in the algorithm where the time for the completion of the considered round is subdivided into 18, 36 and 72 intervals, respectively. However, these small differences do not influence the overall accuracy of the algorithm, which is able to correctly predict the geometry of the ring, for all the tested slices subdivision strategies, with a deviation lower than 2.5%.

Excluding the differences in the calibration round, last four columns of Table 5, where the analytical model is set to reach 800 mm whereas the numerical simulation reaches a final outer diameter of 811.75 mm, the maximum deviation from the numerical simulation is calculated in 2.3% for the 18 slices case, 1.7% for the 36 slices case and 1.17% for the 72 slices case.

Since the analytical algorithm [13] is implemented in an MS Excel spreadsheet, the computation is immediate and no significant differences in the computational time can be seen among the three different cases.

However, the computational time of the combined CAD-analytical model proposed in this paper is directly linked to the number of slices, as it is hereafter explained.

After the calculation of the geometry of the ring, the resulting data are exported and submitted to the CAD algorithm implemented in the Grasshopper plug-in of Rhinoceros 5, as also shown in "Contact geometry estimation utilizing Grasshopper" section of Fig. 2, and the calculation is iterated until the projection of the contact arc onto the y-axis, Fig. 6, is

Table 10 Maximum radial forming force estimations (in [kN]) and error (in percentage)

Case	F_Y [9]	F_Q [10]	F_P [6]	$F_{authors}$	F_{FEM}	e_Y	e_Q	e_P	$e_{authors}$
1	1058	1110	1078	1378	1370	−22.7	−18.9	−21.3	0.61
2	869	908	879	1120	1152	−24.6	−21.2	−23.7	−2.78
3	591	586	571	705	717	−17.5	−14.9	−17.7	−1.62

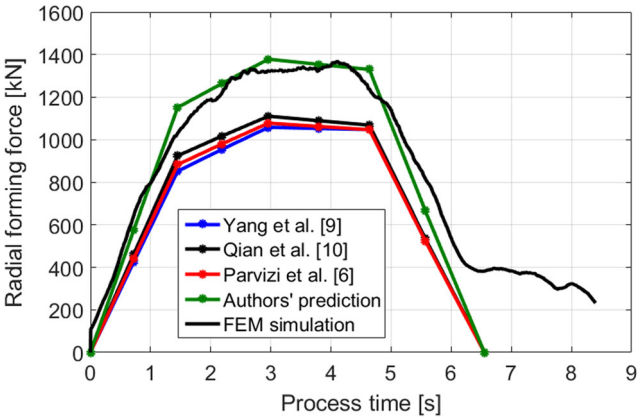

Fig. 20 Radial forming force comparison for Case 1

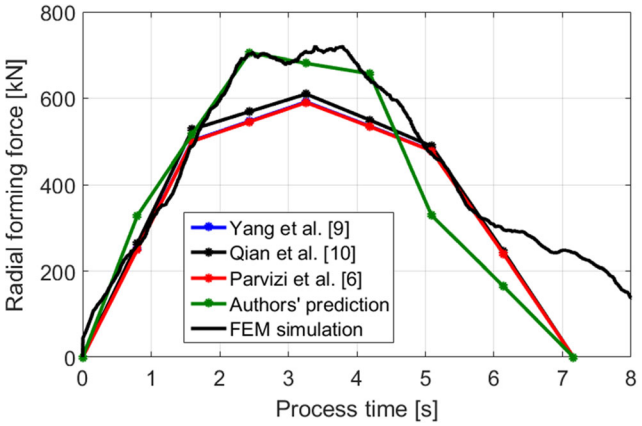

Fig. 22 Radial forming force comparison for Case 3

same on both mandrel and main roll side. This value is considered the result for the projection of the contact arc between the tools of the considered slice in the considered round of the process.

The time required for one single computation, thus for the calculation of the projection of the contact arc for one single slice, is averagely 2.5 s on an i7–6700 3.4GHz processor with 16GB of RAM installed. The small deviations between the calculation times are caused by the proximity of the initial guess solution to the final solution, which is not preconditioned.

When the calculations of all the projection of the contact arcs for all the slices in the considered round are completed, the values are averaged in order to allow the calculation of a unique solution for the radial forming force in the considered round.

Considering once again the study case 1, Table 4, the geometry estimations resulting from the 18, 36 and 72 slices subdivisions, relevant for the 3rd round of the process, have been inputted in the CAD program. Accordingly, the projection of the contact arcs have been estimated and averaged, in order to obtain a unique solution of the radial forming force for the considered round of the process, namely the 3rd one. Finally, the radial forming force has been analytically

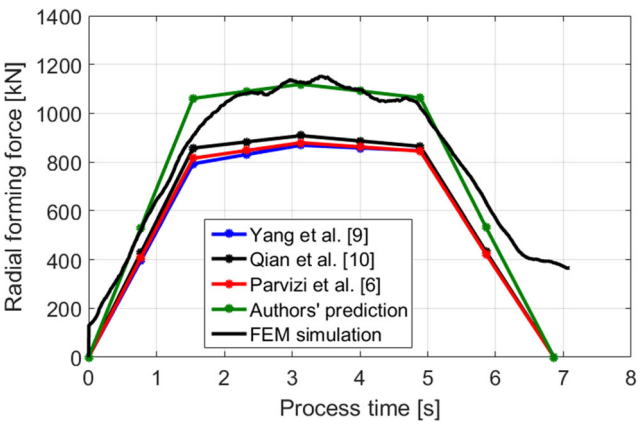

Fig. 21 Radial forming force comparison for Case 2

calculated by utilizing the three different average projections of the projection of the contact arc based on 18, 36 and 72 slices subdivision strategies. The results of the comparison between analytical results, for the three slices subdivision strategies, and the numerical simulation results, are reported in Table 6.

In Table 6, the value of the projection of the contact arc between ring and tools in the numerical simulation have been estimated following the procedure shown in Fig. 13. For each round of the process, four different values have been measured on four different sections of the ring located at 0°, 90°, 180° and 270° with respect to the central axis of mandrel and main roll. In all the cases, the projection of the contact arc in the numerical simulations has been estimated at the center of the ring, along the vertical direction, as shown in Fig. 13.

Based on the results comparison reported in Table 6, the subdivision of the ring into 72 slices results in a considerable increase of the computational time $t_{comp,\,CAD}$ with a light enhance in the estimation of both projection of the contact arc $L_{c,\,CAD}$ and radial forming force $F_{authors}$. For this reason, authors have chosen to utilize the subdivision of the ring into 36 slices for the estimation of the geometries of the ring to be utilized as input for the CAD-analytical model presented in this paper. This subdivision strategy has been utilized for both the validation case, presented in the following section of the paper, as well as for the three study cases reported in Table 4, whore results are summarized in "Result and discussion" section of the paper.

Model validation

In order to validate the proposed approach and the numerical simulation model, laboratory experiments on a ring rolling test machine, Fig. 14, have been carried out.

Being troublesome to operate under hot forming condition and having the test machine a low power on the actuators, in comparison to standard ring rolling machine, the tests have

been carried out in cold forming condition and utilizing a Pb-Sn soft alloy (75% of Pb and 25% of Sn). The material characteristics have been determined by means of compression test and the relevant flow stress curves, measured for different strain rates at room temperature, are presented in following Fig. 15. Additional material properties for the considered Pb75-Sn25 alloy are listed in Table 7.

Concerning the data fitting of the plastic behavior, Eq. (11) is a modification of the one utilized by Kim et al. [20], where the constants relevant for the temperature effects have been neglected since cold forming conditions are considered. The relevant model constants have been derived by inverse calibration from the results of the compression tests, and are reported in Table 8.

In order to compute strain and strain rate to be inputted in the material models for the calculation of the flow stress, previous authors' models detailed in [14, 16] have been utilized. Following the algorithm proposed in [14], the strain tensor in the ring section can be calculated throughout the process. In addition to that, in authors' previous work [16], the equation for the estimation of the contact time between ring and tools in the mandrel-main roll deformation gap is developed and, along with the strain estimation, allows to calculate the strain rate. Both strain and strain rate are computed for each slice of the ring and for each round of the process, allowing to map of the flow stress of the ring throughout the process

$$\sigma_{fs} = K_0(a_0 + \varepsilon)^{a_1}\left(b_0 + \dot{\varepsilon}\right)^{b_1} \tag{11}$$

The technical data of the ring rolling test machine are summarized, along with ring initial and final geometry and additional process conditions, in Table 9. The ring preform, Fig. 16a, has been obtained by melting the Pb-Sn alloy (ingots) in a ring-shaped die and the dimensions have been verified before starting the ring rolling process. The final ring after the ring rolling process is shown in Fig. 16b.

Thanks to a metering roll, always in contact with the outer diameter of the ring and located 180° from the mandrel-main roll deformation gap, the geometrical expansion of the ring is recorded. Moreover, force load-cells are located in the mandrel and the upper axial roll actuators, allowing to acquire the force data during the process. In order to show the reliability of the proposed approach, two different results are presented: the first one, Fig. 17, shows the comparison between analytical estimation, made by utilizing authors' model [13], authors' FEM simulation and laboratory experiment for the ring outer diameter expansion throughout the process. The comparison shows a considerable good agreement among these three results, proving that the kinematic conditions applied in the experiments are well replicated by the FEM simulation as well as by the analytical model.

The latter one, Fig. 18, shows the comparison between the analytical estimation of the radial forming force obtained by utilizing the approach proposed in this paper and the results of the relevant FE simulation and laboratory experiment. Apart from the mechanical and thermal properties related the ring, the numerical model relevant for the validation case has been implemented following the same procedure and features described in the previous section of the paper.

The maximum radial forming force computed in the numerical simulation and that estimated by utilizing the CAD-analytical model proposed in this paper show, respectively, an error of 1.53% and 0.52% in comparison to the experimental results. The cross-comparison among analytical estimation, FEM simulation and experimental results for the proposed validation case show the reliability of the proposed mixed CAD-analytical approach for the estimation of the projection of the contact arc, indirectly verified by the accuracy of the estimation of the radial forming force. Moreover, based on the good agreement between numerical and experimental results, also the developed FEM simulation has shown to be able to replicate well the experimental conditions.

Results and discussion

The choice of targeting the analysis to rings having the final outer diameter of 800 mm is given by the fact that the available literature models have all shown limitations in the analytical estimation of the radial forming force rings of this size. This fact is mainly related to the common concept of estimating an average geometry for the ring for each round of the process, which does not allow accounting for the incremental nature of the ring rolling process. However, in the previous authors' work [13], the geometry of the ring is estimated on a certain number slices and, according to this concepts, each slice has a different geometry than its previous or following one. In addition to that, all the previous literature models assume the thickness draft on the mandrel side to the equal to that on the main roll side, which is not consistent considering that mandrel and main roll diameters are normally different each other.

For the three rings shown in Table 4, by applying the geometry prediction model [13], the strain-strain rate estimation model [14], the temperature model [16] and the force model of Eq. (8) together, the results have shown an underestimation in the prediction of the radial forming, if the literature models [6, 9, 10] for the estimation of the projection of the contact arc are used.

However, if the model described in "Contact geometry estimation utilizing Grasshopper" section is utilized, thanks to a more precise calculation of the projection of the contact arc between ring and tools, the radial forming force can be estimated in a more accurate

way, superseding the limitation shown by the literature models presented in Eqs. (4)–(6).

The precise estimation of the radial forming force, empowered by the combined utilization of the proposed model along with authors' previous ones [13, 14, 16], makes the proposed model to be of interest for both research and industrial environments, since the calculation is performed almost in real-time, and does not require long computational time, as in the case of FEM simulations.

Concerning the estimation of the projection of the contact arc between ring and tools, in the following Fig. 19a, b and c, the evolution of the projection of the contact arc during the rolling time for the three literature models [6, 9, 10], for the proposed authors' model and for the relevant numerical simulation are shown. The comparisons show that the utilization of the three literature models lead to similar estimations of the projection of the contact arc in comparison to the numerical simulation results. However, the developed CAD-analytical model is able to predict quite accurately the numerical results.

By utilizing the estimated projection of the contact arc in the force model presented in previous "Slip line force model" section of the paper, Eq. (8), the evolution of the radial forming force during the rolling time has been estimated for the three study cases of Table 4. In order to promote a fair comparison, for the computation of the force, the same geometrical and flow stress data have been inputted in the force model equation. Accordingly, the differences in the estimations of the radial forming force can be directly attributed to the difference in the estimation of the projection of the contact arc.

As first result concerning the estimation of the radial forming force, in Table 10, the value of the maximum radial forming force, estimated by utilizing the three literature models [6, 0, 10] and that proposed by authors are reported along with the percentage error in comparison to the relevant numerical simulation.

In addition to the results shown Table 10, Figs. 20, 21 and 22 show the prediction of the radial forming force for the whole process time in comparison with the relevant FE simulation. These comparisons show that the proposed approach is not only able to predict the maximum value of the radial forming force but can also catch its trend throughout the process. The small anticipations/delays in the prediction made by the proposed analytical model, shared also by the literature ones, are related to slippage between ring and tools which may happen during the process and which cannot be predicted by the analytical model.

The slippage between ring and tool is an issue related to the torque transfer from the main roll to the ring, which is affected by the friction between these two elements. In the real ring rolling process, slippage may occur for several different reason, either related to the process conditions, such as in the case of a local concentration of lubricant, or due to sudden interference between the ring and the centering rolls, which may cause a loss of contact for a fraction of second. However, being the slippage an unpredictable phenomenon, for this reason, its contribution could not be included in the developed model.

In Fig. 19, the curve of the results obtained by applying the contact arc formulation of Yang et al. [9] and Parvizi et al. [6] are almost overlapped and, for this reason, the difference between the two outcomes is almost not visible.

Conclusion

Thanks to the cross-comparison among analytical, experimental and numerical results, the reliability of the developed mixed CAD-analytical model for the estimation of the projection of the contact arc between ring and tools during the process has been proven. The proposed approach allows estimating the maximum value of the radial forming force with a ± 3% range error, in comparison with the relevant FE simulation and is able to replicate, in a reasonable way, the trend of the forming force curve throughout the process. The comparison among the proposed approach and previous models available in the literature have shown that: i) the result, in terms of radial forming force, are almost equal even utilizing different literature models and that ii) based on the precise estimation of the projection of the contact arc made by utilizing the proposed approach, the radial forming force can be precisely estimated.

In conclusion, the utilization of the proposed approach allows a quick and precise evaluation of the influence of both process parameters and ring geometry on an important output value such as the radial forming force. For this reason, it is of great interest for the process design phase of both research and industrial environments.

Compliance with ethical standards

Conflict of interest The authors declare that they have no conflict of interest.

References

1. Wang ZW, Fan JP, Hu DP, Tang CY, Tsui CP (2010) Complete modeling and parameter optimization for virtual ring rolling. Int J Mech Sci 52(10):1325–1333. https://doi.org/10.1016/j.ijmecsci.2010.06.008
2. Zhou G, Hua L, Qian DS (2011) 3D coupled thermo-mechanical FE analysis of roll size effects on the radial–axial ring rolling process, computational material. Science 50:911–924
3. Guo L, Yang H (2011) Towards a steady forming condition for radial–axial ring rolling. Int J Mech Sci 53:286–299
4. Kim N, Machida S, Kobayashi S (1990) Ring rolling process simulation by the three dimensional finite element method. Int J Mach Tools Manuf 30(4):569–577. https://doi.org/10.1016/0890-6955(90)90008-7

5. Yea Y, Ko Y, Kim N, Lee J (2003) Prediction of spread, pressure distribution and roll force in ring rolling process using rigid–plastic finite element method. J Mater Process Technol 140(1-3):478–486. https://doi.org/10.1016/S0924-0136(03)00721-0
6. Parvizi A, Abrinia K, Salimi M (2011) Slab analysis of ring rolling process assuming constant shear friction. J Mater Eng Perform 20(9):1505–1511. https://doi.org/10.1007/s11665-010-9824-9
7. Parvizi A, Abrinia K (2014) A two-dimensional upper bound analysis of the ring rolling process with experimental results. Int J Mech Sci 79:176–181
8. Mamalis AG, Johnson W, Hawkyard JB (1976) Analyses for roll force and torque in ring rolling, with some supporting experiments. J Mech Eng Sci 18(4):196–208
9. Yang DY, Ryoo JS (1986) An investigation into the relationship between torque and load in ring rolling. J Eng Ind 109(3):190–196
10. Qian DS, Hua L, Pan LB (2009) Research on gripping conditions in profile ring rolling of raceway groove. J Mater Process Technol 209(6):2794–2802. https://doi.org/10.1016/j.jmatprotec.2008.06.033
11. Rhinoceros 5 User's Guide. McNeel & Associates 2016. http://docs.mcneel.com/rhino/5/usersguide/en-us/windows_pdf_user_s_guide.pdf
12. The Grasshopper Primer, Third Ed. V3.3. http://grasshopperprimer.com/en/index.html
13. Berti GA, Quagliato L, Monti M (2015) Set-up of radial-axial ring-rolling process: process worksheet and ring geometry expansion prediction. Int J Mech Sci 99:55–71
14. Quagliato L, Berti GA (2016) Mathematical definition of the 3D strain field of the ring in the radial-axial ring rolling process. Int J Mech Sc 115-116:746–759. https://doi.org/10.1016/j.ijmecsci.2016.07.009
15. Hill R (1950) The mathematical theory of plasticity. Clarendon Press, Oxford
16. Quagliato L, Berti GA (2017) Temperature estimation and slip-line force analytical models for the estimation of the radial forming force in the RARR process of flat rings. Int J Mech Sc 123:311–323. https://doi.org/10.1016/j.ijmecsci.2017.02.008
17. MSC Software Marc® 2015, "Volume B: Element library" technical reference
18. MSC Software Marc® 2015, "Volume C: Program Input" technical reference
19. A. Hensel, T. Spittel, Kraft - und Arbeitsbedarf bildsamer Formgebungsverfahren, 1st edn, Deutscher Verlag für Grundstoffindustrie (1978), Leipzig
20. Kim N, Kim H, Jin K (2012) Optimal design to reduce the maximum load in ring rolling process. Int J Precis Eng Manuf 13(10):1821–1828. https://doi.org/10.1007/s12541-012-0239-4